Myomegalin regulates Hedgehog pathway by controlling PDE4D at the centrosome

Hualing Peng[a,†], Jingyi Zhang[a,†], Amanda Ya[a,‡], Winston Ma[a], Sammy Villa[a], Shahar Sukenik[b], and Xuecai Ge[a,*]

[a]Department of Molecular and Cell Biology and [b]Department of Chemistry and Chemical Biology, University of California, Merced, Merced, CA 95340

ABSTRACT **Mutations in the hedgehog (Hh) signaling are implicated in birth defects and cancers, including medulloblastoma (MB), one of the most malignant pediatric brain tumors. Current Hh inhibitors face the challenge of drug resistance and tumor relapse, urging new insights in the Hh pathway regulation. Our previous study revealed how PDE4D controls global levels of cAMP in the cytoplasm to positively regulate Hh signaling; in the present study, we found that a specific isoform PDE4D3 is tethered to the centrosome by Myomegalin (Mmg), a centrosome/Golgi-associated protein. Mmg loss dislocates PDE4D3 from the centrosome, leading to local PKA overactivation and inhibition of the Hh signaling, leaving other PKA-related pathways unaffected. Mmg loss suppresses the proliferation of granule neuron precursors and blocks the growth of MB in mouse model. Our findings specify a new regulatory mechanism of the Hh pathway and highlight an exciting therapeutic avenue for Hh-related cancers with reduced side effects.**

Monitoring Editor
Karen Oegema
University of California, San Diego

Received: Feb 9, 2021
Revised: May 21, 2021
Accepted: Jul 6, 2021

INTRODUCTION

The Hedgehog (Hh) pathway is widely implicated in birth defects and human tumors (Briscoe and Therond, 2013). One of the Hh-related tumors is medulloblastoma (MB), a malignant pediatric brain tumor (Goodrich *et al.*, 1997). Current treatment of MB, surgery removal followed by chemo- or radiotherapy, brings devastating side effects to the young patients (Fouladi *et al.*, 2005), while the available Hh-pathway inhibitor targeting Smoothened (Smo) is challenged by drug resistance and tumor relapse (Yauch *et al.*, 2009). Therefore, new approaches to inhibit Hh signaling are needed. The Hh signal transduction involves a series of protein transport into and out of the primary cilium and eventually converges on the regulation of Gli transcription factors (Hui and Angers, 2011). Without the ligand Sonic Hh (Shh), the receptor Patched (Ptch) resides in the cilium and prevents the cilium translocation and activation of Smo. On Shh stimulation, Ptch exits the cilium, followed by Smo's accumulation and activation in the cilium. The signaling cascade ultimately activates the transcription activator Gli2 and eliminates the transcription suppressor Gli3R, a proteolytic product from the Gli3 full-length (FL) protein(Wang and Li, 2006; Han and Alvarez-Buylla, 2010). The activated Hh signaling quickly induces the transcription of Gli1, an amplifier of Hh signaling, forming a positive feedback loop.

PKA plays a central role in Hh signaling activation and Gli regulations. PKA phosphorylates Gli3, which primes its further phosphorylation by GSK and CK1. The phosphorylated Gli3 was recognized by the ubiquitin proteosome system that cleaves Gli3FL into Gli3R (Wang and Li, 2006). In addition, PKA also controls Gli2 activation. Within the cell, PKA concentrates at the centrosome (cilium base) where it controls the cilium translocation of Gli2, a step required for Gli2 activation (Tuson *et al.*, 2011). Genetic removal of PKA leads to full activation of the Hh pathway in the developing neural tube (Epstein *et al.*, 1996; Huang *et al.*, 2002; Tuson *et al.*, 2011), further substantiating the strong inhibitory effect of PKA on Hh signaling. Recent studies from the Mukhopadhyay lab suggest that inhibiting

This article was published online ahead of print in MBoC in Press (http://www.molbiolcell.org/cgi/doi/10.1091/mbc.E21-02-0064) on July 14, 2021.

†These authors contribute equally to this work.

‡Current address: Molecular and Cell Biology Graduate Program at Dartmouth College, Hanover, NH 03755.

*Address correspondence to: Xuecai Ge (xge2@ucmerced.edu).

Abbreviations used: AKAR4, A kinase-activity reporter; AOI, area of interest; ECB, extracellular imaging buffer; FBS, fetal bovine serum; FL, full length; FRET, fluorescence resonance energy transfer; GNP, granule neuron precursor; Hh, Hedgehog; KO, knockout; MB, medulloblastoma; MEF, mouse embryonic fibroblast; Mmg, Myomegalin; PAABD, phosphoamino acid-binding domain; PBS, phosphate-buffered saline; PDE, phosphodiesterase; PDE4D, phosphodiesterase 4D; Ptch, Patched; ROI, region of interest; Shh, sonic Hedgehog; Smo, Smoothened; WT, wild type.

the ciliary targeting of adenylyl cyclases, which subsequently reduces cAMP-PKA levels in the cilium, markedly activates Hh signaling in a manner independent of Smo activation (Somatilaka *et al.*, 2020). Conversely, pharmacological activation of PKA inhibits Hh signaling and suppresses Hh-related tumor growth (Yamanaka *et al.*, 2010, 2011). However, PKA is widely involved in many signaling and metabolic pathways; ubiquitous activation of PKA inevitably impacts all signaling pathways. Hence, treatments directly targeting PKA are not practical due to their severe side effects. To avoid these side effects, one feasible strategy is to selectively control PKA activities at the specific subcellular sites where it regulates Hh signaling, leaving other pathways unaffected.

It is known that PKA activity in the cell is compartmentalized by forming complexes that include cAMP-specific phosphodiesterase (PDE) (Zaccolo and Pozzan, 2002; Houslay, 2010; McCormick and Baillie, 2014). In specific compartments, PKA activity is precisely regulated by PDE. In our previous studies, we found that PDE4D, recruited to the cytoplasmic membrane by sema3-Neuropilin signaling, governs cAMP levels in the entire cell to regulate Hh signaling (Hillman *et al.*, 2011; Ge *et al.*, 2015). Our results were corroborated by Williams *et al*. who independently discovered PDE4D as a positive regulator of the Hh pathway in a chemical screen(Williams *et al.*, 2015). Since PKA at the centrosome directly participate in Hh signaling(Barzi *et al.,* 2010; Tuson *et al.*, 2011), can we selectively manipulate PDE4D activity at the centrosome to control local PKA activity? In the current study, we found an approach to dislocate PDE4D3 from the centrosome; the subsequent elevation in local PKA activity suppresses Hh signal transduction and Hh-related tumor growth. Our results highlight an exciting avenue to treat Hh-related cancers with reduced side effects.

RESULTS AND DISCUSSION

Myomegalin (Mmg) interacts with PDE4D3 at the centrosome

To identify an effective approach of selectively modulating cAMP levels at the centrosome, we did a literature search on the subcellular localization of all cAMP-specific PDE. We found that one PDE4D isoform, PDE4D3, was reported to interact with Mmg, a protein associated with the centrosome/Golgi (Verde *et al.*, 2001). But it remains unclear whether PDE4D3 localizes to the centrosome and whether it is involved in the regulation of the Hh signaling. To answer these questions, we first validated the Mmg-PDE4D3 interaction. Mmg is a large protein of 270 kDa, and expressing the FL exogenous protein is ineffective in cells. The previous study identified that the C-terminus of Mmg mediates its interaction with PDE4D3 (Verde *et al.*, 2001) (Figure 1A). We thus fused this domain (Mmg-C) with Flag and expressed it together with HA-PDE4D3 in the cell. We then performed coimmunoprecipitation assay with Flag– and HA–conjugated magnetic beads and found that two proteins coimmunoprecipitated each other (Figure 1B). It is noteworthy that although Flag antibody pulled down significant amount of Flag-Mmg (red triangle in Figure 1B), it only coimmunoprecipitated a small amount of HA-PDE4D3 (red star in Figure 1B), presumably because only a fraction of HA-PDE4D3 in the cell is interacting with Mmg. This is consistent with what we observed in immunostaining results in Figure 1F.

To validate the subcellular localization of Mmg, we stained NIH3T3 cells with the Mmg antibody. As reported before (Roubin *et al.*, 2013), Mmg immunofluorescence partially overlapped with pericentrin, a marker of the centrioles and pericentriolar material (Figure 1C); it also partially overlapped with a Golgi marker GM130 (Figure 1D). We then expressed Flag-Mmg-C in the cell. The majority of Mmg-C colocalized with pericentrin (Figure 1E), suggesting that this domain might mediate Mmg's centrosome localization. When both HA-PDE4D3 and Flag-Mmg-C were expressed in the cell, HA-PDE4D3 overlapped with Flag-Mmg-C at the centrosome/Golgi area, although a significant fraction of HA-PDE4D3 also diffusively distributes to the cytosol (Figure 1F).

A recent study reported that a short isoform of Mmg (aka, Mmg8) that lacks the C-terminus fully overlaps with Golgi marker GM130 (Wang *et al.*, 2014), whereas the C-terminal domain of Mmg almost exclusively localizes to the centrosome (Figure 1E). It is likely that the C-terminal domain of Mmg mediates its localization to the centrosome, while the shorter isoform lacking the C-terminus localizes to the Golgi. The C-terminus also contains the interacting sequence with PDE4D3 (Figure 1A). Taken together, these results suggest that Mmg recruits a small fraction of PDE4D3 from the cytosol to the centrosome.

Mmg loss impairs Hh signal transduction and dislocates PDE4D3 from the centrosome

Next, we tested whether eliminating PDE4D3 from the centrosome impacts the Hh pathway. We silenced Mmg expression with shRNA in NIH3T3 cells, a cell line that contains all components of the Hh pathways and is commonly used to study Hh signaling transduction. Two of the five tested shRNAs significantly reduced the transcript and the protein levels of Mmg (Supplemental Figure S1, A and B). We then treated cells with SAG, a small molecule agonist of the Hh pathway, and assessed the Hh pathway activation with qPCR measuring the transcript level of the Hh target gene Gli1. Mmg shRNA significantly reduced SAG-induced Gli1 expression, indicating that Hh signal transduction was impaired (Supplemental Figure S1C).

To thoroughly eliminate Mmg protein expression, we employed CRISPR/Cas9 to knock out (KO) Mmg in mouse embryonic fibroblasts (MEFs). We choose MEF because it transduces Hh signaling but has a lower ploidy level than NIH3T3 cells. We used two gRNAs targeting the first exon of Mmg and transfected the plasmid containing the two gRNAs and Cas9 into MEF cells, together with EGFP. Single-cell clones were isolated via flow cytometry and expanded (Figure 2A). We obtained two cell clones (#7, #10) of Mmg KO. Both clones appear normal in cell morphology and cell proliferation (data not shown), and the Mmg mRNA and protein levels are undetectable (Figure 2, B and C). Interestingly, among the four alternative splicing isoforms of mouse Mmg (https://www.ncbi.nlm.nih.gov/gene/83679), CRISPR/Cas9 abolished the expression of the longer isoforms (~270 kDa) and spared the shorter isoform (~130 kDa) (Figure 2C), presumably because the shorter isoform uses an alternative transcription starting point. The shorter isoform, however, does not interact with PDE4D3 as it lacks the C-terminus. To identify the INDEL mutations induced by CRISPR/Cas9, we amplified exon 1 and its flanking region with PCR from Mmg KO cells and sequenced individual PCR products. The sequencing results show that three types of mutations were generated in each clone, resulting in a frameshift that eventually leads to nonsense-mediated mRNA decay (Supplemental Figure S2, A–C).

We examined the cilium morphology in Mmg KO cells with immunostaining of a cilium marker, acetylated tubulin. The cilium morphology and length are comparable between wild-type (WT) and Mmg KO cells (Supplemental Figure S3B). The Golgi morphology, assessed by the staining of cis-Golgi marker GM130, is also indistinguishable to WT (Supplemental Figure S3C). To evaluate the Hh signaling in Mmg KO clones, we stimulated cells with SAG and detected Gli1 expression with qPCR and Western blot.

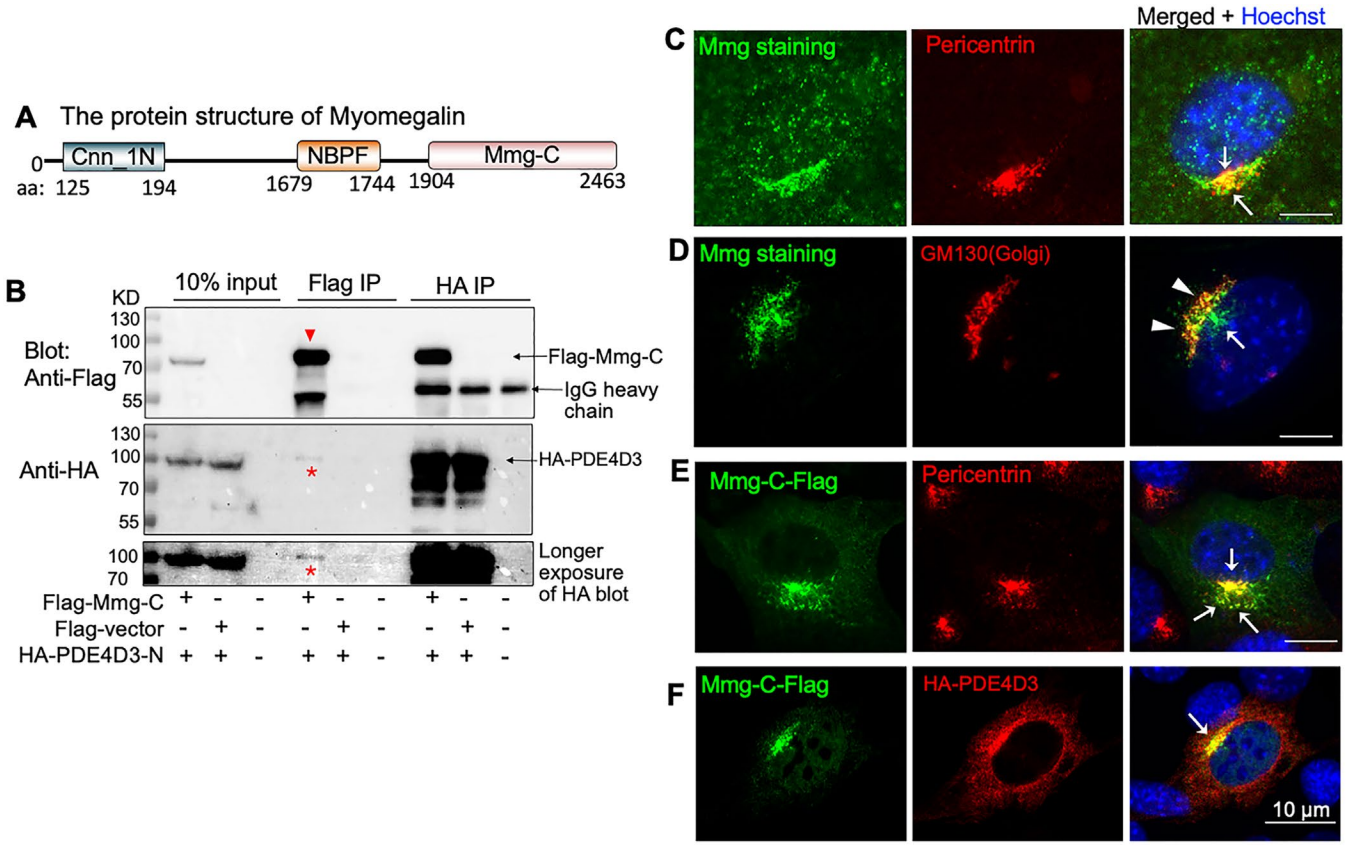

FIGURE 1: PDE4D3 interacts with Mmg at the centrosome. (A) Protein structure of Mmg. Cnn_1N, Centrosomin N-terminal motif 1; NBPF (DUF1220), domain of neuroblastoma breakpoint family; Mmg-C, the domain previously shown to interact with PDE4D3. (B) When overexpressed in HEK293T cells, HA-PDE4D3 and Flag-Mmg C-terminus coimmunoprecipitated with each other, suggesting the interaction of the two proteins. (C, D) Immunostaining of endogenous Mmg in NIH3T3 cells shows that Mmg partially overlaps with pericentrin, a marker for the centrosome and pericentriolar materials (white arrows), and with the Golgi marker GM130 (white triangle). (E) When expressed in NIH3T3 cells, Mmg-C mainly colocalizes to the centrosome and pericentriolar material (white arrows). (F) When expressed in NIH3T3 cells, HA-PDE4D3 diffusively distribute to the cytoplasm, but a significant fraction of PDE4D3 colocalizes with Mmg to the centrosome and pericentriolar material (white arrows).

SAG-induced Gli1 expression was dramatically reduced at the transcript and protein levels in both Mmg KO cell clones (Figure 2, D and E). These results suggest a blockage of Hh transduction after Mmg loss.

Next, we determined the impact of Mmg loss on PDE4D3 localization at the centrosome. Due to the high similarity between PDE4D isoforms, the antibody specific to PDE4D3 is unavailable. Therefore, we expressed very low levels of EGFP-PDE4D3 in Mmg KO cells to mimic the endogenous protein. As expected, in WT cells PDE4D3 shows significant overlap with pericentrin, in addition to its diffusive localization to other subcellular sites (Figure 2F). However, in Mmg KO cells, the intensity of PDE4D3 at the centrosome is significantly reduced (Figure 2, F and G). Therefore, without Mmg, PDE4D3 is dislocated from the centrosome.

Our CRISPR/Cas9 only abolishes the expression of Mmg FL that contains the C-terminus, sparing the shorter isoforms. C-terminus mediates Mmg localization to the centrosome, whereas the shorter isoform localizes to the Golgi. This may explain why Golgi morphology is intact in our Mmg CRISPR/Cas9 KO cells (Supplemental Figure S3C), whereas in these cells PDE4D3 is dislocated from the centrosome (Figure 2F). In summary, our data suggest that loss of Mmg markedly suppresses Hh signal transduction, and dislocates PDE4D3 from the centrosome.

Mmg loss selectively increases local PKA activity at the centrosome and reduces the IBMX-mediated potentiation of PKA activity

Dislocation of PDE4D3 from the centrosome increases local cAMP levels, which may eventually lead to PKA overactivation. To confirm this, we employed two methods to evaluate local PKA activity at the centrosome. First, to measure the basal levels of active PKA, we stained cells with an antibody that recognizes active PKA (phospho-PKA T197). This antibody has been used to evaluate PKA activity in previous studies (Barzi *et al.*, 2010; Tuson *et al.*, 2011; Ge *et al.*, 2015). We highlighted the centrosome and pericentriolar areas with pericentrin staining and measured the phospho-PKA levels in this area in ImageJ. As expected, the centrosomal active PKA levels are much higher in Mmg KO cells compared with those in WT MEF (Figure 3, A and B). Further, expressing exogenous Mmg-C in Mmg KO cells restored active PKA levels to normal (Figure 3B). This change of PKA activity, however, is limited locally to the centrosome, since the overall phospho-PKA levels remain the same in Mmg KO cells (Figure 3C). In addition, we detected the phosphorylation levels of CREB, the cytosolic substrate of PKA (Shaywitz and Greenberg, 1999). The phospho-CREB (S133) levels show no difference between WT and Mmg KO cells (Figure 3C). Thus, Mmg loss increased the basal PKA activity selectively at the centrosome.

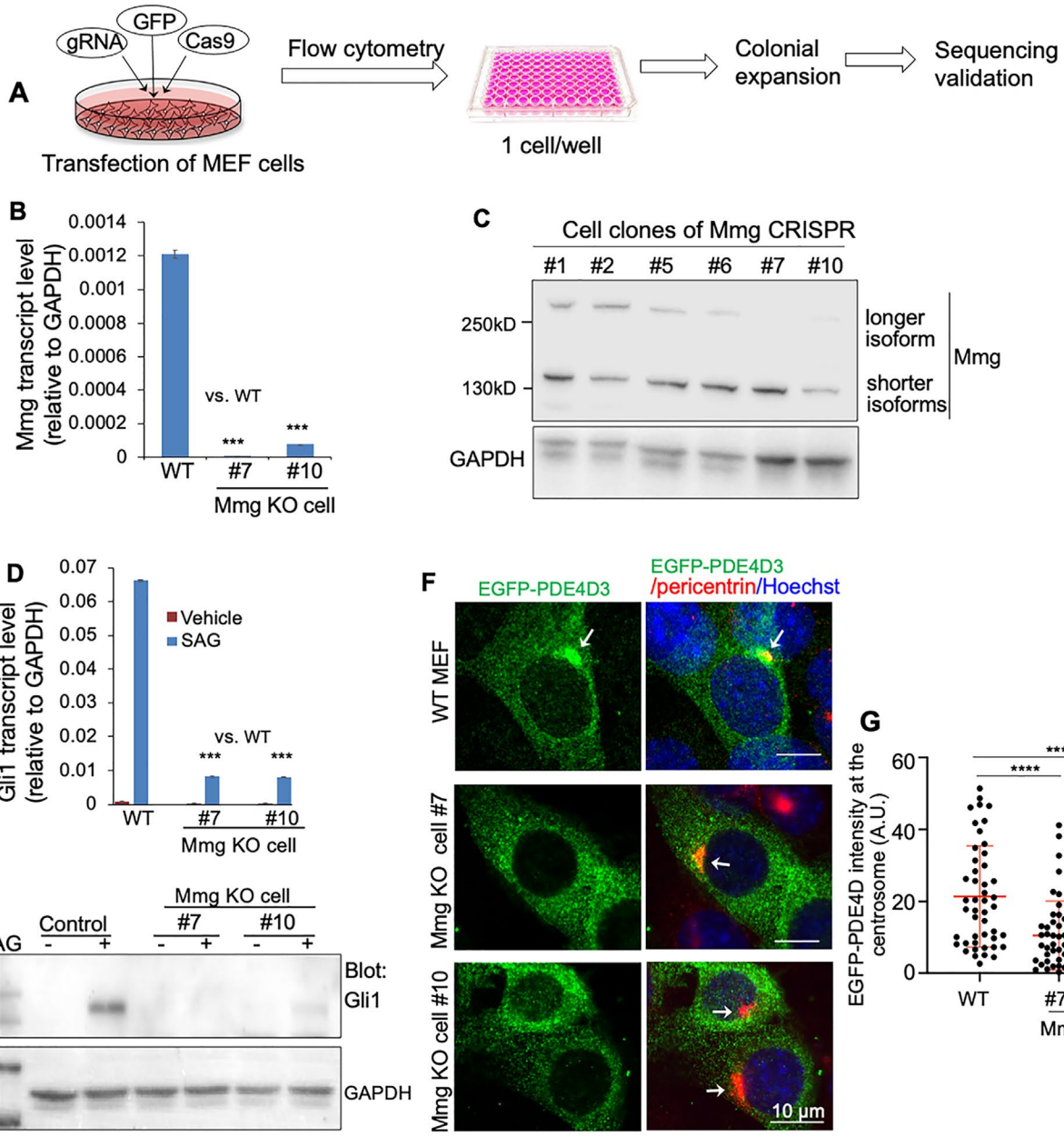

FIGURE 2: Mmg KO dislocates PDE4D from the centrosome and impairs Hh signal transduction. (A) Procedure of generating Mmg CRISPR cell clones. Thirty cell clones were established and tested for Mmg transcript levels and protein levels. (B) In two of the Mmg CRISPR cell clones, the transcript of Mmg was hardly detectable by qPCR. (C) Western blot shows that in cell clones #7 and #10, the CRISPR abolished the expression of the longer isoforms of Mmg, but the shorter isoform remains unaffected. (D, E) Mmg CRISPR KO clones were stimulated with SAG for 24 h, and Hh signaling activity was evaluated by Gli1 transcript levels and protein levels. Graphs in B and D show mean ± SD, $n = 3$ biological replicates, $^{***}p < 0.001$, unpaired Student's t test. (F) Representative images of EGFP-PDE4D3 expressed in WT or Mmg KO cell clones. PDE4D3 concentrates at the centrosome and pericentriolar material in WT cells (white arrow); however, in CRISPR cell clones, it only exhibits diffusive distribution to the cytoplasm and lacks the significant overlap with pericentrin (white arrows). (G) Quantification of PDE4D intensity at the centrosome. Results shown are from one of the two independent experiments. Graphs show mean ± SD, 50–70 cells are quantified for each condition. $^{***}p < 0.001$, $^{****}p < 0.0001$, Kruskal–Wallis nonparametric one-way ANOVA, followed by Dunn's multiple comparison. A.U.: arbitrary unit.

Second, we monitored the dynamic PKA activity in live cells with A kinase-activity reporter (AKAR4), a fluorescence resonance energy transfer (FRET)-based PKA probe developed in Jin Zhang's lab (Zhang *et al.*, 2001; Herbst *et al.*, 2011). In this probe, a FRET pair (CFP and YFP) is connected by a linker sequence that contains PKA phosphorylation sites and a phosphoamino acid-binding domain (PAABD). PKA phosphorylation induces conformational changes in the linker, which brings the FRET pair in close proximity to efficiently produce FRET (Figure 3D). To target AKAR4 to the centrosome, we fused it with the regulatory subunit of PKA (PKARIIα), a protein predominantly localized to the centrosome (Zhang *et al.*, 2001). As expected, when RIIα-AKAR4 is expressed in MEF, the probe is

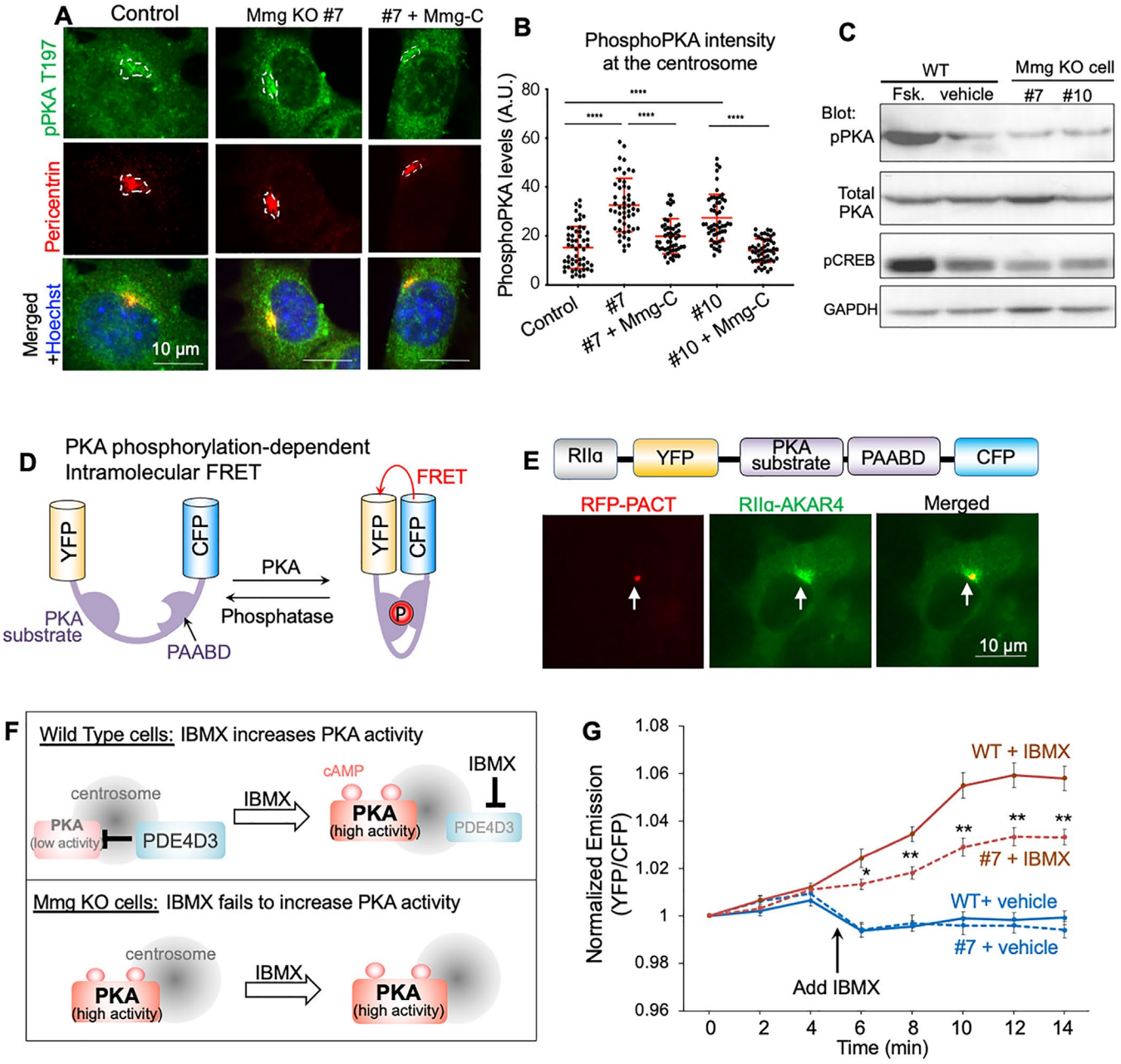

FIGURE 3: Mmg loss increases PKA activity at the centrosome and reduces the IBMX-mediated potentiation of PKA activity. (A) Representative images of phospho-PKA staining in WT, Mmg KO, and Mmg-C overexpressing cells. Dotted lines circles the areas where pPKA intensity was measured based on the staining of pericentrin. (B) Quantification of phospho-PKA intensity at the centrosome; 50–70 cells are quantified for each condition. Data are shown as mean ± SD. Statistics: Kruskal–Wallis nonparametric one-way ANOVA, followed by Dunn's multiple comparison. ***$p < 0.001$, ****$p < 0.0001$. A.U.: arbitrary unit. (C) Western blot shows that the global levels of active PKA do not change in Mmg KO cells. Forskolin (Fsk) treatment serves as a positive control of PKA overactivation in the entire cell. (D) Schematic view of AKAR4, a FRET-based probe for PKA activity. The CFP (Cerulean) and YFP (cpVE172) are linked by a linker sequence that contain a PKA phosphorylation site and a PAABD. PKA phosphorylation induces conformational change in the linker, which brings CFP and YFP in close proximity to produce FRET. (E) By fusing AKAR4 to the RII subunit of PKA, we targeted the probe to the centrosome. Immunostaining results confirmed the centrosome localization of RIIα-AKAR4. (F) Diagram showing that inhibiting PDE4D increases PKA activity in WT cells, but has little effect on PKA activity in Mmg KO cells. (G) Normalized emission of FRET acceptor over donor before and after IBMX 0.1 mM. The ratio of YFP/CFP at each time point was normalized to time 0; $n = 8–13$ cells for each condition. Data are shown as mean ± SEM. Statistics: *t* test between the WT cells and Mmg KO cells at the same time point. *$p < 0.05$, **$p < 0.01$.

concentrated at the centrosomal area (Figure 3E). The centrosome is marked by coexpression of RFP-PACT (Gillingham and Munro, 2000).

As the number of AKAR4 proteins incorporated to the centrosome varies from cell to cell, it is impractical to directly compare the basal levels of FRET signal between cells. However, within the same

cell, the FRET signal can be compared over time. We therefore normalized the FRET signal in individual cells to time 0. We treated cells with IBMX, a PDE inhibitor that is commonly used to elevate cAMP levels and PKA activities in the cell (Zhang *et al.*, 2001; Herbst *et al.*, 2011). Since PDE4D3 is dislocated from the centrosome in Mmg KO cells and the local PKA activity is constitutively high, we hypothesize that IBMX's effect will be compromised at the centrosome in Mmg KO cells (Figure 3F). To test this hypothesis, we analyzed FRET efficiency (YFP/CFP) at the centrosome before and after IBMX treatment (Figure 3G and Supplemental Figure S4). In WT cells, IBMX gradually increased FRET efficiency, peaking at 12 min. In contrast, Mmg KO significantly dampened FRET efficiency at all time points (Figure 3G). Taken together, Mmg loss dislocates PDE4D3 from the centrosome, thereby promoting the local basal PKA activity that cannot be further elevated by the PDE inhibitor.

It is also noteworthy that after adding IBMX, FRET was not completely abolished in Mmg KO cells, indicating the existence of other PDE isoforms at the centrosome (Figure 3G). PDE4D is a large protein family comprising more than 12 alternative splicing isoforms in mammalian cells (Maurice *et al.*, 2014). It will be intriguing for future studies to delineate the identify of these PDE isoforms and their targeting mechanism to the centrosome.

Mmg loss promotes Gli3R production and blocks Gli2 transportation to the cilium tip

The transcription factor Gli2 and Gli3 are PKA substrates in the Hh pathway. After PKA phosphorylation, Gli3 is proteolytically processed into Gli3R, a transcription repressor (Figure 4A). On Hh signaling activation, the Gli3 processing ceases and Gli3R levels markedly reduce (Wang and Li, 2006; Humke, Dorn, Milenkovic, Scott, and Rohatgi, 2010; Tukachinsky, Lopez, and Salic, 2010; Hui and Angers, 2011). We examined Gli3 processing by Western blot. In WT cells, SAG treatment reduced Gli3R levels by 40%. In contrast, SAG stimulation had minimal impact on Gli3R levels in Mmg KO cells. (Figure 4, B and C). Meanwhile, the unstimulated Mmg KO cells exhibit Gli3R levels slightly higher, but not statistically significant, compared to those in WT cells. After SAG stimulation, the Gli3R levels in Mmg KO cells are significantly higher compared to those in WT cells. These results suggest that without Mmg, the overactive PKA at the centrosome promotes the processing of Gli3 FL into Gli3R, and Mmg KO cells remain insensitive to SAG stimulation.

PKA affects the proteolysis of Gli2 only very slightly but more dramatically controls its accumulation at cilia tips, a step required for Gli2 activation (Barzi *et al.*, 2010; Tuson *et al.*, 2011). We therefore examined the levels of Gli2 at the cilia tips after SAG stimulation. The Gli2 intensity at the cilium tips in Mmg KO cells was significantly lower, compared with that in WT cells (Figure 4D). When exogenous Mmg was expressed in KO clones, the Gli2 level at the cilium tips was restored (Figure 4, D and E). Therefore, Mmg loss overactivates PKA at the centrosome, which blocks Gli2 transport and activation at the cilium tip, leading to inhibition of the Hh signaling.

In summary, our data suggest a model of how Mmg and PDE4D3 at the centrosome control local PKA activity to regulate the Hh pathway. Without Shh, PKA activity at the centrosome is high due to high local cAMP levels. The centrosomal cAMP may be produced in the cilium by proteins such as GPR16 (Mukhopadhyay *et al.*, 2013), or is diffused to the centrosome from other cytosolic areas. After Shh stimulation, GPR161 exits the cilium and stops the cAMP production; the cAMP diffused to the centrosome from nearby cytosolic areas is degraded by PDE4D3. The inactive PKA at the centrosome allows Gli2 to be translocated and activated in the cilium tips and stops Gli3R production, leading to Hh pathway activation (Figure 4F). In Mmg KO cells, PDE4D3 is dislocated from the centrosome, the cAMP diffused from the nearby areas is not effectively degraded, and the PKA activity remains high in both Hh-unstimulated and -stimulated conditions. This high PKA activity suppresses Gli2 activation and keeps Gli3R levels high and subsequently blocks the activation of Hh signaling (Figure 4G).

Targeting PDE4D3 to the centrosome rescued Hh signaling in Mmg KO cells

Our data suggest that Mmg loss dislocates PDE4D3 from the centrosome, which subsequently elevates local PKA activity to suppress Hh signaling. To further strengthen the link between the centrosomal PDE4D3 and Hh signaling, we restored PDE4D3 to the centrosome by expressing PACT-Flag-PDE4D3 in Mmg KO cells (Supplemental Figure S5A). We hypothesize that restoring PDE4D3 to the centrosome will suppress local PKA activity and rescue Hh signaling in Mmg KO cells. To test it, we electroporated PACT-Flag-PDE4D3 in Mmg KO cells, and induced Hh signaling with SAG. We then assessed Hh signaling activity with qPCR measuring the transcript level of the Hh target gene Gli1. PACT-Flag-PDE4D3 significantly increased SAG-induced Gli1 expression in Mmg KO cells, indicating that Hh signaling was rescued (Supplemental Figure S5B).

Next, we measured the intensity of phospho-PKA T197 at the centrosome in Mmg KO cells that express PACT-Flag-PDE4D3. The results show that restoring centrosomal PDE4D3 decreased phospho-PKA intensity to a level similar to that in WT cells (Supplemental Figure S5, C and D). To test the effect of local PKA activity on Gli2 transport, we measured Gli2 intensity at the cilium tip in PACT–Flag–PDE4D3-transfected cells. Our results show that the Gli2 levels are significantly increased compared to those of the nontransfected cells, and the Gli2 intensities are comparative to those in WT cells (Supplemental Figure S5, E and F). As a conclusion, targeting PDE4D3 to the centrosome rescued Hh signaling in Mmg KO cells.

Mmg loss blocks cell proliferation in primary cultured granule neuron precursors (GNPs)

In the developing cerebellum, Shh is the mitogen that stimulates GNP proliferation (Dahmane and Ruiz i Altaba, 1999; Wallace, 1999; Wechsler-Reya and Scott, 1999). Overactive Hh signaling leads to GNP overproliferation that eventually results as MB, one of the most malignant pediatric brain tumor (Kool *et al.*, 2012). In situ hybridization results show that both PDE4D3 and Mmg (www.informatics.jax.org/image/MGI:5332354, www.informatics.jax.org/image/MGI:5333985) are highly expressed in the developing cerebellum (Richter *et al.*, 2005); it is likely that the mechanism of Mmg-PDE4D3 regulation on Hh pathway applies to the control of GNP proliferation. To test this hypothesis, we cultured GNPs from P7 mouse neonates in dishes and infected GNPs with lentiviral particles expressing shRNA against Mmg (shRNA #99) (Figure 5A). GNP proliferation was induced by SAG. After 3 d of primary culture, GNP proliferation was assessed by BrdU incorporation assay. As expected, Mmg shRNA significantly reduced Mmg transcript levels and reduced the rate of BrdU incorporation after pulse labeling (Figure 5, B–D). Hh signal activity was significantly reduced in Mmg knockdown cells, demonstrated by decreased transcript levels of Gli1, a Hh target gene (Figure 5E). In summary, our results suggest that the same mechanism of Hh signaling regulation by Mmg-PDE4D3 may control GNP proliferation in the developing cerebellum.

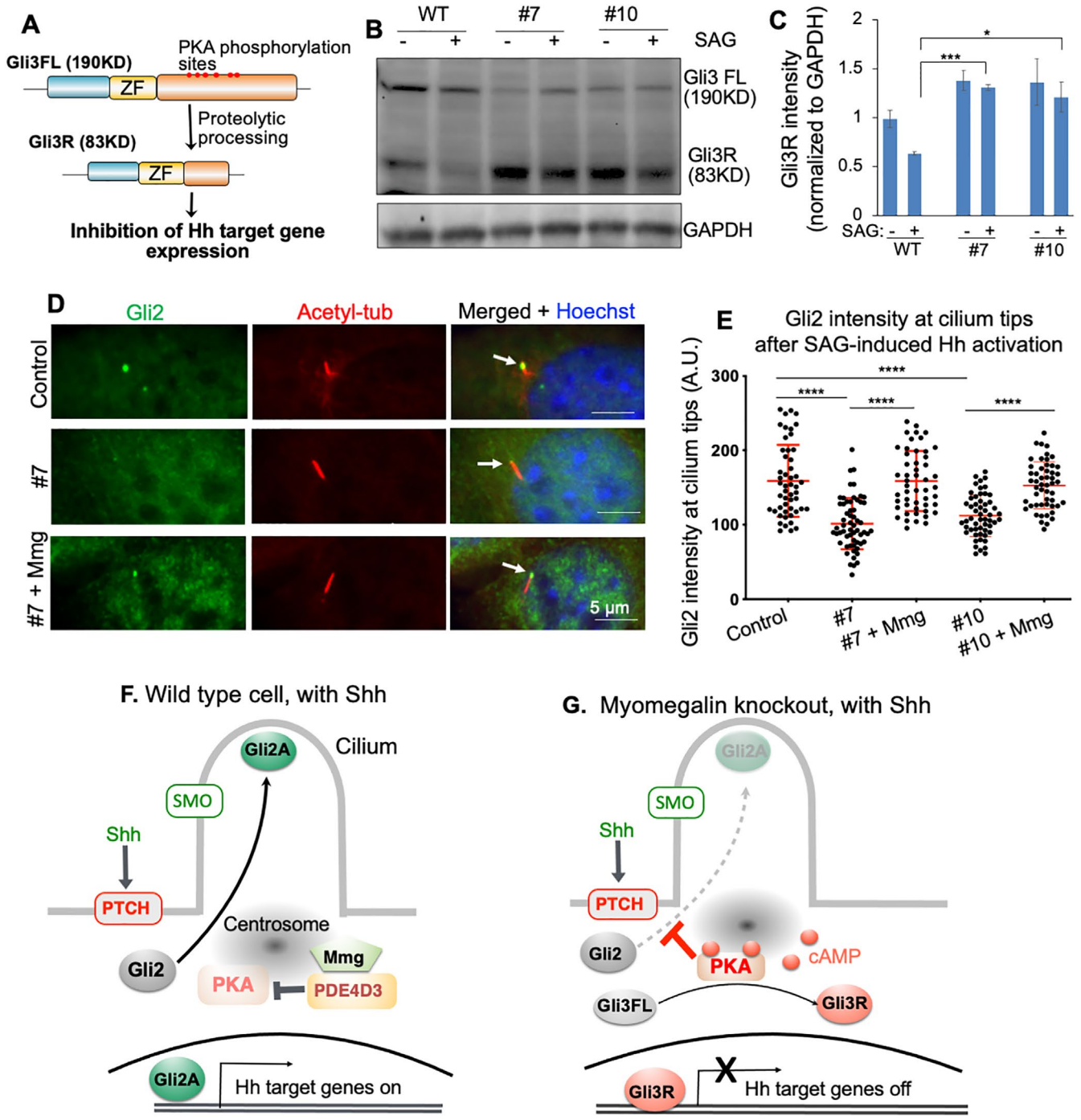

FIGURE 4: Mmg loss impacts Gli3 processing and Gli2 transportation to the cilium tips. (A) The diagram showing the proteolytic processing of Gli3 after PKA phosphorylation. (B) Twenty-four hours of SAG treatment reduced Gli3R levels in WT cells, but not in Mmg KO cell clones. (C) Quantification of Gli3R levels from three independent experiments. Data are shown as mean ± SE. Statistics: unpaired Student *t* test. *$p < 0.05$, ***$p < 0.001$. (D) Representative images of Gli2 immunostaining after cells are stimulated with SAG. White arrows point to Gli2 at the cilium tips. (E) Quantification of Gli2 levels at the cilium tips. Mmg KO reduced Gli2 levels at the cilium tips, while Mmg overexpression restored Gli2 intensity; 50–70 cells are quantified for each condition. Results shown are from one of two independent experiments. Data are shown as mean ± SD. Statistics: Kruskal–Wallis nonparametric one-way ANOVA, followed by Dunn's multiple comparison. ****$p < 0.0001$. A.U.: arbitrary unit. (F, G) Diagram showing PED4D3 specifically controls PKA activities at the centrosome to regulate the Hh signaling transduction. Under normal conditions, on Shh stimulation, SMO is translocated and activated in the cilium, which then triggers a signaling cascade that reduces cAMP levels at the cilium base. The subsequent inhibition of PKA allows Gli2 to be translocated and activated in the cilium tips (F). Without Mmg, PDE4D3 is dislocated from the centrosome and fails to degrade the local cAMP. Thus, PKA levels remain high at the centrosome even after Shh stimulations. Hyperactive PKA suppresses Gli2 activation and promotes Gli3R production. As a result, the Hh pathway cannot be activated (G).

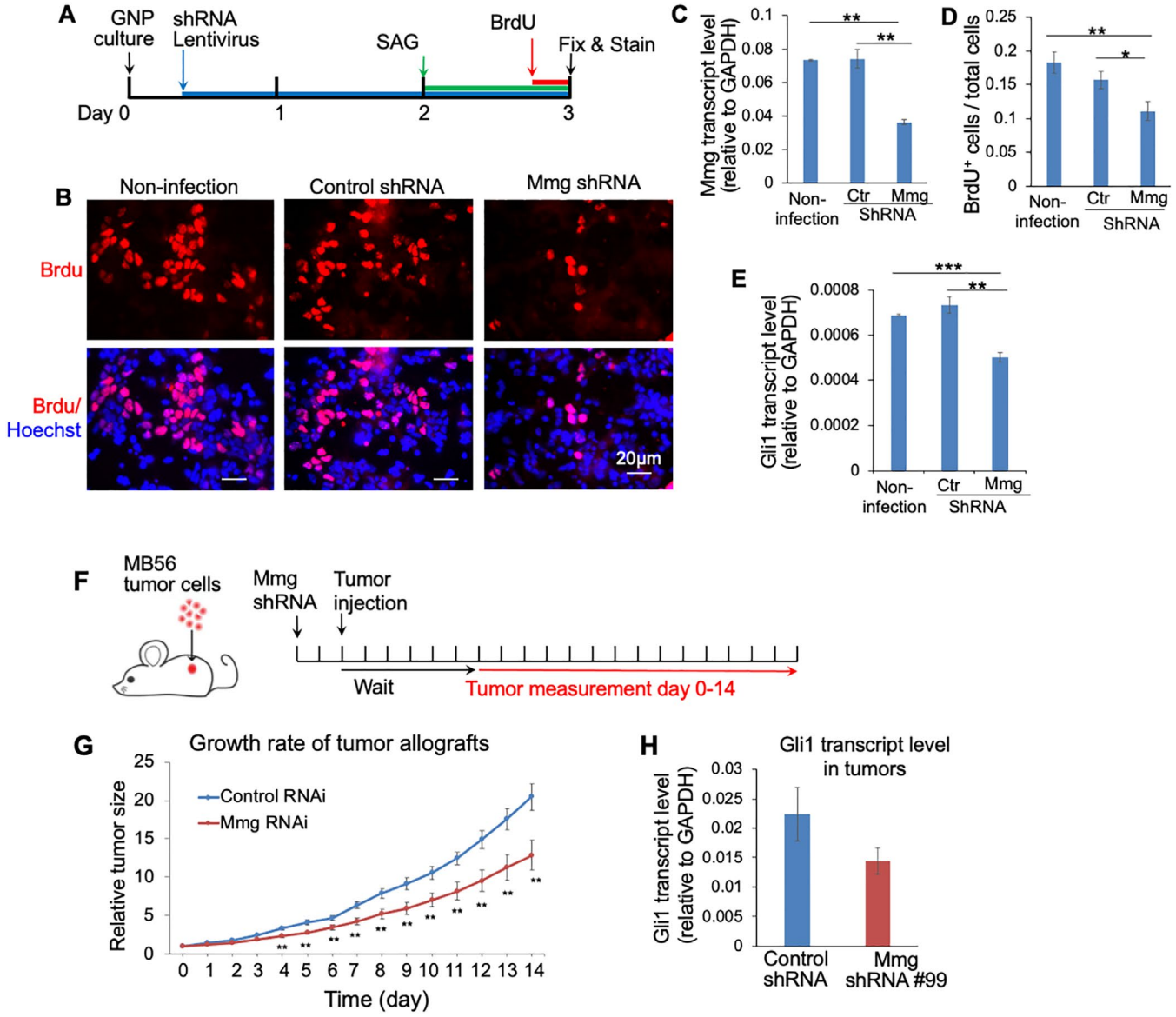

FIGURE 5: Mmg knockdown blocked cell proliferation in primary cultured GNPs and suppressed the growth rate of MB in mouse model. (A) Schematic of BrdU incorporation assay in primary cultured GNPs. Lentivirus expressing shRNA against Mmg or control shRNA was added to the cell 5–6 h after GNPs were plated in dishes. SAG was added to the culture 24 h before cells were fixed. BrdU pulse labeling lasted for 4 h right before cells were fixed. (B) Representative images of BrdU immunostaining in GNPs. (C) Mmg transcript levels at the end of the experiments, measured by qPCR. (D) BrdU incorporation rate in GNPs. (E) Levels of Hh signaling activity evaluated by Gli1 transcript levels. Graphs in C–E show mean ± SD, $n = 3$ biological repeats, unpaired Student's t test, $^*p < 0.05$, $^{**}p < 0.01$. Results in D represent quantification from three slides, and from each slide four areas were randomly chosen for quantification. (F) Schematic diagram of the MB56 tumor allograft experiment in mouse. Measurement started 6 days after tumor allograft when the size of tumors could be accurately measured. (G) The relative tumor size is defined as the tumor volume on the indicated day divided by that on day 0. For each treatment, eight to nine mice were used, and each mouse was transplanted with two tumors on their hind flank. Results shown are from one of the two independent experiments. (H) At the end of the experiment, the Gli1 transcript levels in six of randomly sampled tumors were assessed by qPCR. Hh signaling activity was reduced by Mmg RNAi. Data are presented as mean ± SEM. Statistics: Student's t test. $^*p < 0.05$, $^{**}p < 0.01$, $^{***}p < 0.001$.

Mmg loss reduced the growth rate of MB in the mouse model

Next, we assess the effect of Mmg loss on the Hh-related tumor growth in the mouse model of MB subcutaneous allograft used in our previous studies (Ge *et al.*, 2015). We employed MB56, MB tumor cells directly taken from a Ptch$^{+/-}$ mouse, the first and well-established MB mouse model (Goodrich *et al.*, 1997; Purzner *et al.*, 2018). We infected MB56 with lentiviral particles that express Mmg (shRNA #99) or control shRNA; 2 d after infection, tumor cells were injected subcutaneously in the hind flank of nude mice. Six days after injection, tumor size was measured daily for 2 wk (Figure 5F). We found that Mmg loss significantly slowed tumor growth starting from day 4 of measurement (Figure 5G). At the end of the experiment, we evaluated Gli1 levels in randomly sampled tumors and

found that Mmg loss significantly reduced Hh signal activity (Figure 5H). Thus, knockdown of Mmg suppressed the growth of Hh-related tumors.

Our study pointed to an effective method to suppress Hh signaling in cancers. Current Hh inhibitors target Smo, and these inhibitors are facing challenges of drug resistance and tumor relapse (Yauch *et al.*, 2009). Since the Mmg-PDE4D-PKA axis acts directly at Gli transcription factors, downstream of Smo, targeting this axis will be effective for cancers that have developed resistance to Smo inhibitors. Further, it is known that the basal activity of PDE4D is high, and most PDE4D small molecular inhibitors act by blocking the catalytic domain of PDE4D (Gavaldà and Roberts, 2013). These inhibitors block all PDE4D isoforms and are associated with severe side effects. Our results suggest that we may eliminate PDE4D activity specifically from the centrosome without blocking its catalytic domain. It pinpointed an effective therapeutic avenue to treat Hh-related cancers with reduced side effects.

Hh signaling could influence PKA localization in some systems. A recent study on neural progenitors in the chicken embryonic neural tube shows that high Hh signaling is correlated to the symmetric recruitment of PKA to the replicated centrosomes in dividing cell. This symmetric PKA distribution is required to maintain symmetric proliferative division of the progenitor cells (Saade *et al.*, 2017). This study showed that when PKA-RII, the subunit that binds to and inhibits PKA catalytic subunit, is targeted to the centrosome, Hh signal is enhanced (Figure 8f in Saade *et al.* 2017). This is consistent with the well-established role of PKA as an inhibitor of Hh signaling and with our current study about the impact of centrosomal PKA activity on Hh signaling.

Cells have evolved two mechanisms to accurately govern local levels of cAMP and PKA activity: 1) controlling its production by adenylyl cyclase and 2) managing its degradation by cAMP-specific PDEs. We believe that activation of Hh signaling involves both mechanisms. The first mechanism has been shown to be mediated by GPR161 that resides at the cilium. When the Hh pathway is off, GPR161 activates the Gαs-adenylyl cyclase pathway and keeps the local cAMP levels high (Mukhopadhyay *et al.*, 2013). On Shh stimulation, GPR161 exits the cilium and stops cAMP production (Mukhopadhyay *et al.*, 2013). Synergistic to this mechanism, PDE4D at the centrosome degrades the cAMP that is diffused from the nearby subcellular areas. The combined effects of these two mechanisms keep local PKA activities in check to allow the ensuing Hh signaling events to occur. When PDE4D activity is absent from the centrosome, the local cAMP concentration fails to reduce to the subthreshold level, even though the GPR161-Gαs-adenylyl cyclase pathway stops to produce cAMP. As a result, the high PKA levels at the centrosome suppresses the Hh signal transduction. Our study unmasked the roles of centrosomal PDE4D in the Hh pathway.

MATERIALS AND METHODS

Request a protocol through *Bio-protocol*.

Plasmids and generation of Mmg KO CRISPR cell clones

Human PDE4D3 was generously provided by the Marco Conti lab at the University of California, San Francisco and was subcloned to include HA and EGFP tag. Mmg-C was cloned by RT-PCR with a mouse total mRNA library and subcloned to include Flag and EGFP tag. The FRET probe AKAR4 was generously provided by the Jin Zhang lab (available in Addgene). The pcDNA3-mPKA-RIIα-AKAR4-NES was constructed by linking mPKA-RIIα with AKAR4-NES. The linker sequence is GGGGSGS. The two gRNA were designed via the Guide Design Resources of the Feng Zhang lab at the Massachusetts Institute of Technology (https://zlab.bio/guide-design-resources). The two gRNAs were cloned into the backbone of pX330-U6-Chimeric_BB-CBh-hSpCas9 (Addgene 42230) and transfected into MEF cells together with EGFP via lipofectamine 2000; 48 h after transfection, EGFP-positive cells were sorted by flow cytometer and plated into individual wells in a 96-well plate. Individual cell clones were cultured for 2–4 wk and transferred to a 24-well plate for further expansion.

Time-lapse image with AKAR4

MEF cells were cotransfected with RIIα-AKAR4 and RFP-PACT via electroporation and cultured in DMEM supplemented with 10% fetal bovine serum (FBS) at 37°C; 24 h later, cells were plated onto an 8-chambered lab-Tex II coverglass (ThermoFisher) at a density of 3.5×10^4/well and then grown for approximately 24 h before imaging.

For imaging, cells were washed once with extracellular imaging buffer (ECB, 5 mM KCl, 125 mM NaCl, 1.5 mM $CaCl_2$, 1.5 mM $MgCl_2$, 10 mM glucose, 20 mM HEPES) and kept in ECB in the dark at room temperature. Images were collected with an epifluorescence microscope (Zeiss Observer3) with a 40× dry 0.9 NA objective lens connected to two linked Hamamatsu Flash v3 sCMOS cameras to facilitate real-time FRET imaging. The CFP fluorophore was excited using a 430-nm LED (Colibi7, Zeiss), and emission was collected using a triple-bandpass emission filter, 467/24 + 555/25 + 687/145 (set 91 HE from Zeiss). Downstream, the collected emission was further split onto the two cameras using a 520-nm dichroic. Exposure time was set for 200 ms. Images were acquired every 2 min. IBMX was added to the cell as indicated in the experiment.

FRET analysis

Results were analyzed in ImageJ. The centrosome was identified in red channel via RFP-PACT and selected as a region of interest (ROI). An automated, stack-based thresholding was built on the Renyi entropy method to identify strong fluorescence in the RFP channel throughout the time course. Intensities of the CFP and YFP at each time point in the ROI were measured. To control for different expression levels of AKAR, intensity at each time point was normalized to time 0.

Western blot

Cells were lysed on ice in RIPA buffer containing 25 mM Tris-HCl (pH 7.6), 150 mM NaCl, 1% NP-40, 1% sodium deoxycholate, 0.1% SDS, 1 mM PMSF, 10 mM sodium fluoride, 2 mM sodium pyrophosphate, 1 mM sodium orthovanadate, Roche protease inhibitor cocktail, and Roche PhosSTOP inhibitor cocktail for 30 min. Lysates were cleared with centrifugation at 13,000 rpm for 30 min at 4°C. Protein concentrations of the supernatants were determined with a BCA protein assay kit (Pierce). Protein samples were boiled in 6× SDS sample buffer for 10 min and resolved in SDS–PAGE. Protein binds were transferred to PVDF membrane (88520, ThermoFisher), which were blocked in Tris buffer (pH 7.0) containing 0.1% Tween-20 and 5% bovine serum albumin. The membrane was incubated in primary antibodies (diluted in blocking buffer) overnight at 4°C and washed 3× before incubation with HRP–conjugated secondary antibodies. Protein bands were visualized with ECL Western Blot substrate (Pierce, 32109).

Primary antibodies used were mouse anti-GAPDH (ab9484, Abcam), rabbit anti-phospho-PKA-T197 (5661S, Cell Signaling), rabbit anti-phospho-CREB-S133 (9198S, Cell Signaling), mouse anti-PKA (610625, BD Biosciences), rabbit anti-Gli1 (V812, Cell Signaling), and rabbit anti-Mmg (PA5-30324, Invitrogen).

Coimmunoprecipitation

Plasmids were transfection into HEK293Tcells with lipofectamine 2000 reagent (Invitrogen) according to the manufacturer's instructions. Plasmids used were HA-PDE4D3, 3xFlag-Mmg-C560 and 3xFlag-vector (E4026, Sigma, MO); 24 h after transfection, cells were lysed in ELB buffer (150 mM NaCl, 1% Triton X-100, 50 mM Tris, pH 8.0, 5 mM EDTA, 5 mM NaF, 2 mM Na_3VO_4) supplemented with Protease inhibitor cocktail (Roche 11836170001) for 30 min at 4°C. Lysates were cleared by centrifugation at 14,000 rpm for 15 min. Protein concentration of supernatants was determined using Pierce BCA Protein Assay Kit (Thermo Scientific). Equal amounts of protein were loaded to the anti-Flag M2 Magnetic beads (M8823, Sigma) and anti-HA Magnetic beads (88836, Thermo Scientific) and incubated for 1 h at room temperature. Beads were washed according to manufacturer's instruction and incubated with 2× Laemmli sample buffer at 95°C for 5 min. Samples were loaded to 10% SDS–PAGE gel and Western blot was performed. Antibodies used were HA-tag rabbit antibody (3724S, Cell Signaling) and anti-Flag M2 antibody (F1804, Sigma).

Immunofluorescence staining

NIH3T3 or MEF cells were grown on poly-D-lysine (A003E, Sigma)-coated coverslips they were close to full confluency and serum-starved overnight. Cells were fixed with 4% paraformaldehyde for 10 min at room temperature. Cells were then blocked with 2% donkey serum and 0.1% triton in phosphate-buffered saline (PBS) for 1 h. Primary and secondary antibodies were incubated with cells in the blocking buffer. Images were taken with LEICA DMi8 microscopy, or a Zeiss LSM880 confocal microscope, with a 60× oil lens.

Primary antibodies used were anti-Flag M2 antibody (F1804, Sigma), anti-mouse Pericentrin (611814, BD Biosciences), anti-rabbit Mmg antibody (PA552969, Invitrogen), anti-rabbit GFP antibody (A11122, ThermoFisher), mouse anti-acetylated tubulin (T6793, SIGMA), goat anti-Gli2 (AF3635, R&D SYSTEMS), and rabbit anti-pPKA (ab59218, Abcam).

Quantification of Phospho-PKA, PDE4D3, and Gli2

The levels of phospho-PKA and EGFP-PDE4D3 in the centrosome were measured using ImageJ software as follows. first, an area of interest (AOI) was delineated based on the signal intensity of pericentrin staining; second, the mean gray value in AOI was measured in the phospho-PKA or EGFP-PD4D3 channel (F1); third, the contour of AOI was manually dragged to a nearby region within the cell, and the mean gray value of the enclosed area was measured as background (F2). The final values of phospho-PKA and PDE4D3 were calculated as $F = F1–F2$.

To quantify Gli2 levels at the cilium tips, the contour of the cilium tips was outlined in red channel (acetylated tubulin staining). The mean gray density in the enclosed area was measured in green channel (Gli2 staining). The background gray density was measured and subtracted to obtain the final Gli2 intensity at the cilium tips.

For each condition, 35–60 cells were measured. In the Mmg rescue experiment, only cells that were transfected with EGFP-Mmg were measured. Data analysis was done with Graphpad Prism 8.0 Software. Kruskal–Wallis nonparametric one-way ANOVA was used for statistical analysis.

Quantitative PCR

Cells were plated in 6-well plates at 0.5×10^6 cells per well and cultured overnight. For Hh induction, cells were stimulated with 100 nM SAG in starvation medium (0.5% FBS in DMEM) for 20–24 h. Total RNAs were isolated with Trizol reagent. The concentration of total RNA was normalized, and the same amount of RNA was mixed with qScript XLT-1 Step, RT-qPCR ToughMix (Quantabio 66149433), together with specific TaqMan expression assays. The real-time PCR is performed in QuantStudio 3 (ThermoFisher).

The following TaqMan gene expression probes used were Mm00494654_g1 (Gli1), Mm00626240_m1 and Mm01257004_m1 (Mmg), and Mm99999915_g1 (GAPDH).

Primary culture of GNPs and Brdu incorporation assay

A neonate CD1 mice was sacrificed at P7. The cerebellum was taken out and cut into small pieces with razor blades and incubated at 37°C for 15 min in digestion buffer (HBSS with 20 mM HEPES, pH 7.3, supplemented with trypsin and DNase I). At the end of incubation, the digestion buffer was aspirated and replaced with neurobasal medium with 250 U/ml DNase I. Tissues were then triturated with pipet tips and polished Pasteur pipettes. After seated for 2 min, dissociated cells were collected from the upper layer and centrifuged at 1000 rpm for 5 min. Cells were washed one time and resuspended in neurobasal, supplemented with B27 (17504044, Life Technologies), Glutamax, and 1% penicillin/streptomycin. Cells were then plated on coverslips coated with poly-D-lysine and laminin. Lentivirus expressing Mmg shRNA were added 5 h after plating and incubated overnight; 48 h after plating, 10 nM SAG was added to the cells and incubated overnight. Brdu (20 μM) was added to the culture and pulse labeled for 4 h, after which cells are fixed with 4% paraformaldehyde. Brdu immunostaining were performed with mouse-anti-Brdu antibody (662411Ig, Proteintech).

MB allograft mouse model

All of the in vivo surgery steps and treatments were performed in accordance with the animal protocols approved by UC Merced's Institutional Biosafety Committee (IACUC). MB56 tumor cells were cultured in neurobasal medium supplemented with B-27 (21103-049, ThermoFisher). Cells were infected with lentiviral particles of shRNA against Mmg or control shRNA; 48 h later, cells were then collected, centrifuged, and resuspended in PBS at 2×10^7cells per 50 μl; 50 μl cells were mixed with Matrigel (354234, ThermoFisher) at a 1:1 volume ration. The 100-μl mixture was slowly injected into the hind flanks of 8–10 nude mice of 7 wk (002019, Jackson Laboratory) under isoflurane anesthesia; 6 d after injection, the tumor volume was measured daily with digital calipers for 2 wk. At the end of the experiments, mice were killed and five to six tumors were harvested randomly. Tumor tissues were proceeded to RNA extraction and qPCR. To generate a tumor growth curve, the relative tumor size is calculated as the ration of tumor size on each day over the size of the same tumor on day 1 of measurement.

Quantification and Statistical Analysis

Statistical analysis was performed using Graphpad Prism 8.0 Software (Graphpad Software; La Jolla, CA). Statistical significance was determined by Student's *t* test or Kruskal–Wallis nonparametric one-way ANOVA as mentioned in the figure legends.

ACKNOWLEDGMENTS

We thank Marco Conti for their generous gifts of PDE4D constructs, and helpful discussions. We thank Lavpreet Jammu, Anh Diep, and Christi Waer for initial characterization of Mmg shRNA and for generating Mmg and PDE4D3 constructs. We thank Lin Gan for helpful discussions on the manuscript. The research was supported by National Institutes of Health Grant R15 CA235749 to X.G.

REFERENCES

Barzi M, Berenguer J, Menendez A, Alvarez-Rodriguez R, Pons S (2010). Sonic-hedgehog-mediated proliferation requires the localization of PKA to the cilium base. J Cell Sci 123, 62–69.

Briscoe J, Therond PP (2013). The mechanisms of Hedgehog signalling and its rolesin development and disease. Nat Rev Mol Cell Biol 14, 416.

Dahmane N, Ruiz i Altaba A (1999). Sonic hedgehog regulates the growth and patterning of the cerebellum. Development 126, 3089–3100.

Epstein DJ, Marti E, Scott MP, McMahon AP (1996). Antagonizing cAMP-dependent protein kinase A in the dorsal CNS activates a conserved Sonic hedgehog signaling pathway. Development 122, 2885–2894.

Fouladi M, Gilger E, Kocak M, Wallace D, Buchanan G, Reeves C, Robbins N, Merchant T, Kun LE, Khan R, *et al.* (2005). Intellectual and functional outcome of children 3 years old or younger who have CNS malignancies. J Clin Oncol. https://doi.org/10.1200/JCO.2005.01.214

Gavaldà A, Roberts RS (2013). Phosphodiesterase-4 inhibitors: a review of current developments (2010–2012). Expert Opin Ther Pat 23, 997–1016.

Ge X, Milenkovic L, Suyama K, Hartl T, Purzner T, Winans A, Meyer T, Scott T, MP LE (2015). Phosphodiesterase 4D acts downstream of Neuropilin to control Hedgehog signal transduction and the growth of medulloblastoma. eLife 4, e07068.

Gillingham AK, Munro S (2000). The PACT domain, a conserved centrosomal targeting motif in the coiled-coil proteins AKAP450 and pericentrin. EMBO Rep 1, 524–529.

Goodrich LV, Milenkovic L, Higgins KM, Scott MP (1997). Altered neural cell fates and medulloblastoma in mouse patched mutants. Science, 277, 1109–1113. http://www.ncbi.nlm.nih.gov/pubmed/9262482

Han Y-G, Alvarez-Buylla A (2010). Role of primary cilia in brain development and cancer. Curr Opin Neuroviol 20, 58–67.

Herbst KJ, Allen MD, Zhang J (2011). Spatiotemporally regulated protein kinase A activity is a critical regulator of growth factor-stimulated extracellular signal-regulated kinase signaling in PC12 cells. Mol Cell Biol 31, 4063–4075.

Hillman TR, Feng BY, Ni J, Woo WM, Milenkovic L, Hayden-Gephart MG, Teruel MN, Oro AE, Chen JK, Scott MP (2011). Neuropilins are positive regulators of Hedgehog signal transduction. Genes Dev. https://doi.org/10.1101/gad.173054.111

Houslay MD (2010). Underpinning compartmentalised cAMP signalling through targeted cAMP breakdown. Trends Biochem Sci. https://doi.org/10.1016/j.tibs.2009.09.007

Huang Y, Roelink H, McKnight GS (2002). Protein kinase A deficiency causes axially localized neural tube defects in mice. J Biol Chem 277, 19889–19896.

Hui C, Angers S (2011). Gli proteins in development and disease. Annu Rev Cell Dev Biol 27, 513–537.

Humke EW, Dorn KV, Milenkovic L, Scott MP, Rohatgi R (2010). The output of Hedgehog signaling is controlled by the dynamic association between Suppressor of Fused and the Gli proteins. Genes Dev. https://doi.org/10.1101/gad.1902910

Kool M, Korshunov A, Remke M, Jones DTW, Schlanstein M, Northcott PA, Cho YJ, Koster J, Schouten-Van Meeteren A, Van Vuurden D, *et al.* (2012). Molecular subgroups of medulloblastoma: An international meta-analysis of transcriptome, genetic aberrations, and clinical data of WNT, SHH, Group 3, and Group 4 medulloblastomas. Acta Neuropathologica 123, 473–484.

Maurice DH, Ke H, Ahmad F, Wang Y, Chung J, Manganiello VC (2014). Advances in targeting cyclic nucleotide phosphodiesterases. Nat Rev Drug Discov 13, 290–314.

McCormick K, Baillie GS (2014). Compartmentalisation of second messenger signalling pathways. Curr Opin Genet Dev 27, 20–25.

Mukhopadhyay S, Wen X, Ratti N, Loktev A, Rangell L, Scales SJ, Jackson PK (2013). The ciliary G-protein-coupled receptor Gpr161 negatively regulates the sonic hedgehog pathway via cAMP signaling. Cell 152, 210–223.

Purzner T, Purzner J, Buckstaff T, Cozza G, Gholamin S, Rusert JM, Hartl TA, Sanders J, Conley N, Ge X, *et al.* (2018). Developmental phosphoproteomics identifies the kinase CK2 as a driver of Hedgehog signaling and a therapeutic target in medulloblastoma. Sci Signal https://doi.org/10.1126/scisignal.aau5147

Richter W, Jin S-LC, Conti M (2005). Splice variants of the cyclic nucleotide phosphodiesterase PDE4D are differentially expressed and regulated in rat tissue. Biochem J 388(Pt 3), 803–811.

Roubin R, Acquaviva C, Chevrier V, Sedjai F, Zyss D, Birnbaum D, Rosnet O, Sedjaï F, Zyss D, Birnbaum D, *et al.* (2013). Myomegalin is necessary for the formation of centrosomal and Golgi-derived microtubules. Biol Open 2, 238–250.

Saade M, Gonzalez-Gobartt E, Escalona R, Usieto S, Martí E (2017). Shh-mediated centrosomal recruitment of PKA promotes symmetric proliferative neuroepithelial cell division. Nat Cell Biol 19, 493–503.

Shaywitz AJ, Greenberg ME (1999). CREB: A stimulus-induced transcription factor activated by a diverse array of extracellular signals. Annu Rev Biochem. https://doi.org/10.1146/annurev.biochem.68.1.821

Somatilaka BN, Hwang SH, Palicharla VR, White KA, Badgandi H, Shelton JM, Mukhopadhyay S (2020). Ankmy2 prevents smoothened-independent hyperactivation of the hedgehog pathway via cilia-regulated adenylyl cyclase signaling. Dev Cell 54, 710–726.e8.

Tukachinsky H, Lopez LV, Salic A (2010). A mechanism for vertebrate Hedgehog signaling: Recruitment to cilia and dissociation of SuFu-Gli protein complexes. J Cell Biol. https://doi.org/10.1083/jcb.201004108

Tuson M, He M, Anderson KV (2011). Protein kinase A acts at the basal body of the primary cilium to prevent Gli2 activation and ventralization of the mouse neural tube. Development, 138, 4921–4930.

Verde I, Pahlke G, Salanova M, Zhang G, Wang S, Coletti D, Onuffer J, Jin SLC, Conti M (2001). Myomegalin is a novel protein of the golgi/centrosome that interacts with a cyclic nucleotide phosphodiesterase. J Biol Chem 276, 11189–11198.

Wallace VA (1999). Purkinje-cell-derived Sonic hedgehog regulates granule neuron precursor cell proliferation in the developing mouse cerebellum. Curr Biol 9, 445–448.

Wang B, Li Y (2006). Evidence for the direct involvement of βTrCP in Gli3 protein processing. Proc Natl Acad Sci USA 103, 33–38.

Wang Z, Zhang C, Qi RZ (2014). A newly identified myomegalin isoform functions in Golgi microtubule organization and ER-Golgi transport. J Cell Sci 127, 4904–4917.

Wechsler-Reya RJ, Scott MP (1999). Control of neuronal precursor proliferation in the cerebellum by sonic hedgehog. Neuron, 22, 103–114.

Williams CH, Hempel JE, Hao J, Frist AY, Williams MM, Fleming JT, Sulikowski GA, Cooper MK, Chiang C, Hong CC (2015). An in vivo chemical genetic screen identifies phosphodiesterase 4 as a pharmacological target for hedgehog signaling inhibition. Cell Rep 11, 43–50.

Yamanaka H, Oue T, Uehara S, Fukuzawa M (2011). Hedgehog signal inhibitor forskolin suppresses cell proliferation and tumor growth of human rhabdomyosarcoma xenograft. J Pediatr Surg. https://doi.org/10.1016/j.jpedsurg.2010.11.010

Yamanaka H, Takaharu O, Uehara S, Fukuzawa M (2010). Forskolin, a Hedgehog signal inhibitor, inhibits cell proliferation and induces apoptosis in pediatric tumor cell lines. Mol Med Rep. https://doi.org/10.3892/mmr-00000230

Yauch RL, Dijkgraaf GJP, Alicke B, Januario T, Ahn CP, Holcomb T, Pujara K, Stinson J, Callahan CA, Tang T, *et al.* (2009). Smoothened mutation confers resistance to a Hedgehog pathway inhibitor in medulloblastoma. Science 326, 572–574.

Zaccolo M, Pozzan T (2002). Discrete microdomains with high concentration of cAMP in stimulated rat neonatal cardiac myocytes. Science 295, 1711–1715.

Zhang J, Ma Y, Taylor SS, Tsien RY (2001). Genetically encoded reporters of protein kinase A activity reveal impact of substrate tethering. Proc Natl Acad Sci 98, 14997–15002.